Three-dimensional rearrangement of single atoms using actively controlled optical microtraps

Woojun Lee, Hyosub Kim, and Jaewook Ahn*

Department of Physics, KAIST, Daejeon 305-701, South Korea

**jwahn@kaist.ac.kr*

Abstract: We propose and demonstrate three-dimensional rearrangements of single atoms. In experiments performed with single ^{87}Rb atoms in optical microtraps actively controlled by a spatial light modulator, we demonstrate various dynamic rearrangements of up to $N = 9$ atoms including rotation, 2D vacancy filling, guiding, compactification, and 3D shuffling. With the capability of a phase-only Fourier mask to generate arbitrary shapes of the holographic microtraps, it was possible to place single atoms at arbitrary geometries of a few μm size and even continuously reconfigure them by conveying each atom. For this purpose, we loaded a series of computer-generated phase masks in the full frame rate of 60 Hz of the spatial light modulator, so the animation of phase mask transformed the holographic microtraps in real time, driving each atom along the assigned trajectory. Possible applications of this method of transformation of single atoms include preparation of scalable quantum platforms for quantum computation, quantum simulation, and quantum many-body physics.

OCIS codes: (020.7010) Laser trapping; (350.4855) Optical tweezers or optical manipulation; (090.2890) Holographic optical elements; (270.5585) Quantum information and processing; (020.3320) Laser cooling; (070.6120) Spatial light modulators.

References and links

1. J. E. Bjorkholm, R. R. Freeman, A. Ashkin, and D. B. Pearson, "Observation of focusing of neutral atoms by the dipole forces of resonance-radiation pressure," Phys. Rev. Lett. **41**, 1361–1364 (1978).
2. S. Chu, J. E. Bjorkholm, A. Ashkin, and A. Cable, "Experimental observation of optically trapped atoms," Phys. Rev. Lett. **57**, 314–317 (1986).
3. J. I. Cirac and P. Zoller, "A scalable quantum computer with ions in an array of microtraps," Nature **404**, 579–581 (2000).
4. S. Bergamini, B. Darquie, M. Jones, L. Jacubowiez, A. Browaeys, and P. Grangier, "Holographic generation of microtrap arrays for single atoms by use of a programmable phase modulator," J. Opt. Soc. Am. B **21**, 1889–1894 (2004).
5. F. K. Fatemi, M. Bashkansky, and Z. Dutton, "Dynamic high-speed spatial manipulation of cold atoms using acousto-optic and spatial light modulation," Opt. Express **15**, 3589–3596 (2007).
6. X. He, P. Xu, J. Wang, and M. Zhan, "Rotating single atoms in a ring lattice generated by a spatial light modulator," Opt. Express **17**, 21007–21014 (2009).
7. F. Nogrette, H. Labuhn, S. Ravets, D. Barredo, L. Béguin, A. Vernier, T. Lahaye, and A. Browaeys, "Single-atom trapping in holographic 2D arrays of microtraps with arbitrary geometries," Phys. Rev. X **4**, 021034 (2014).
8. J. Beugnon, C. Tuchendler, H. Marion, A Gaëtan, Y. Miroshnychenko, Y. R. P. Sortais, A. M. Lance, M. P. A. Jones, G. Messin, A. Browaeys, and P. Grangier, "Two-dimensional transport and transfer of a single atomic qubit in optical tweezers," Nat. Phys. **3**, 696–699 (2007).
9. S. Kuhr, W. Alt, D. Schrader, M. Müller, V. Gomer, and D. Meschede, "Deterministic delivery of a single atom," Science **293**, 278 (2001).

#260694 Received 8 Mar 2016; revised 14 Apr 2016; accepted 22 Apr 2016; published 27 Apr 2016

10. M. P. MacDonald, L. Paterson, K. Volke-Sepulveda, J. Arlt, W. Sibbett, and K. Dholakia, "Creation and manipulation of three-dimensional optically trapped structures," Science **296**, 1101–1103 (2002).
11. Y. Miroshnychenko, W. Alt, I. Dotsenko, L. Förster, M. Khudaverdyan, D. Meschede, D. Schrader, and A. Rauschenbeutel, "An atom-sorting machine," Nature **442**, 151 (2006).
12. M. J. Piotrowicz, M. Lichtman, K. Maller, G. Li, S. Zhang, L. Isenhower, and M. Saffman, "Two-dimensional lattice of blue-detuned atom traps using a projected Gaussian beam array," Phys. Rev. A **88**, 013420 (2013).
13. N. Schlosser, G. Reymond, and P. Grangier, "Collisional blockade in microscopic optical dipole traps," Phys. Rev. Lett. **89**, 023005 (2002).
14. T. Xia, M. Lichtman, K. Maller, A. W. Carr, M. J. Piotrowicz, L. Isenhower, and M. Saffman, "Randomized benchmarking of single-qubit gates in a 2D array of neutral-atom qubits," Phys. Rev. Lett. **114**, 100503 (2015).
15. I. Buluta, S. Ashhab, and F. Nori, "Natural and artificial atoms for quantum computation," Rep. Prog. Phys. **74**, 104401 (2000).
16. O. Mandel, M. Greiner, A. Widera, T. Rom, T. W. Hänsch, and I. Bloch, "Controlled collisions for multi-particle entanglement of optically trapped atoms," Nature **425**, 937–940 (2003).
17. I. Bloch, "Ultracold quantum gases in optical lattices," Nat. Phys. **1**, 23–30 (2005).
18. M. Schlosser, S. Tichelmann, J. Kruse, and G. Birkl, "Scalable architecture for quantum information processing with atoms in optical micro-structures," Quant. Inf. Proc. **10**, 907–924 (2011).
19. H. Dammann and K. Görtler, "High-efficiency in-line multiple imaging by means of multiple phase holograms," Opt. Commun. **3**, 312–315 (1971).
20. T. Grünzweig, A. Hilliard, M. McGovern, and M. F. Andersen, "Near-deterministic preparation of a single atom in an optical microtrap," Nat. Phys. **6**, 951–954 (2010).
21. D. McGloin, G. C. Spalding, H. Melville, W. Sibbett, and K. Dholakia, "Applications of spatial light modulators in atom optics," *Opt. Express* **11**, 158–166 (2003).
22. H. Kim, W. Lee, H.-g. Lee, H. Jo, Y. Song, and J. Ahn, "In situ single-atom array synthesis by dynamic holographic optical tweezers," http://arxiv.org/abs/1601.03833
23. A. Jechow, E. W. Streed, B. G. Norton, M. J. Petrasiunas, and D. Kielpinski, "Wavelength-scale imaging of trapped ions using a phase Fresnel lens," Opt. Lett. **36**, 1371–1373 (2011).
24. R. W. Bowman, G. M. Gibson, A. Linnenberger, D. B. Phillips, J. A. Grieve, D. M. Carberry, S. Serati, M. J. Miles, and M. J. Padgett, "Red Tweezers: Fast, customisable hologram generation for optical tweezers," Comput. Phys. Commun. **185**, 268–273 (2014).
25. F. O. Fahrbach, F. F. Voigt, B. Schmid, F. Helmchen, and J. Huisken, "Rapid 3D light-sheet microscopy with a tunable lens," Opt. Express **21**, 21010–21026 (2013).

1. Introduction

Optical dipole trapping is a simple and powerful technique for holding and steering atoms in space [1, 2]. This technique, recently developing to far off-resonant optical trapping (FORT), utilizes the electric dipole interaction force exerted by light to manipulate the external degrees of freedom of quantum objects. From a pre-cooled atom ensemble, focused laser beams can capture and isolate single atoms without inducing optical transitions, so their internal states are well preserved in the electronic ground state up to several seconds, which makes the optically trapped single atoms a promising candidate for storing and processing quantum information [3]. Currently there is a strong interest for using the FORT in engineering scalable quantum platforms [4–13], because the manipulation of N single atoms in a synthetic structure of a few μm size is a crucial necessity for the study of quantum computation, quantum simulation, and quantum many-body physics [14–17].

Optical dipole microtraps and optical lattices [17] are the well-known tools for atom arrays. In the context of the manipulation and control of individual atoms in an array, optical microtraps are considered to be a versatile tool, having many control parameters. The optical microtraps have been achieved by various methods, including micro lens arrays [18], diffractive optical elements such as Dammann grating [19], spatial light modulators (SLM) [5–7], optical standing waves [11], and dynamic light deflectors [5]. With these methods, adiabatic transport of atoms in one and two dimensions [8, 9], atom sorting with a cross junction [11], collisional blockade mechanism [13], controlled collisions for near-deterministic atom loading [20], atom array rotations [6], and single-qubit gate arrays [14] have been demonstrated. These impressive achievements are currently being geared towards a deterministically-loaded high-dimensional

#260694 Received 8 Mar 2016; revised 14 Apr 2016; accepted 22 Apr 2016; published 27 Apr 2016

arbitrary architecture of N single atoms in which the the internal and external degrees of freedom of the atoms are freely controllable.

Holographic methods of using a programmable SLM in the Fourier domain have been a work horse in the construction and manipulation of various forms of two-dimensional (2D) microtrap arrays [7]. The SLM phase pattern generation for $N_{tr} \sim 2N$ optical microtraps is often performed with iterative Fourier transform algorithms (IFTA) [7]. However, because of the frame-to-frame intensity flickering [21], dynamic and simultaneous control of N single atoms with a series of IFTA-gererated patterns has remained difficult. Recently we devised a simple method for flicker-free atom controls with optical microtraps [22]. In this paper, we extend this method further to achieve 3D rearrangements of N singe atoms. We experimentally demonstrate holographic methods for various 2D and 3D transformations of single atoms in an array.

In the remaining sections, we first describe in Sec. 2 the principle of the dynamic and simultaneous displacement of N_{tr} optical microtraps in 3D. The transverse and axial displacements are programmed with linear and quadratic phase gradients of the SLM pixels, respectively. In Sec. 3 we explain the experimental setup and the control and imaging procedure. The experimental demonstrations of various 2D and 3D atom-array rearrangements are presented in Sec. 4, before the conclusion in Sec. 5.

2. Phase pattern generation for 3D displacement

The flicker-free frame-to-frame evolution of microtraps in 3D is implemented with phase patterns programmed in the Fourier domain. The transverse displacement $(\Delta x, \Delta y)$ is implemented by a linear phase gradient [22] and the axial displacement Δz by a Fresnel lens phase [23]. The linear phase $e^{i(k_X X + k_Y Y)}$, where (X,Y) is the position in the Fourier domain and (k_X, k_Y) the transverse wave vector, makes the focal spot of a beam shifted by $(\Delta x, \Delta y) = (k_X f_o, k_Y f_o)/k$ from the optic axis (the z axis), where k is the wavenumber of the beam, when the beam is focused by an objective lens with focal length f_o [see Fig. 1(a)]. Also, when the beam passes through a Fresnel lens with focal length f_{F} and then focused by the same f_o lens which is f_o apart from the Fresnel lens, after relaying 4-f geometry [see Fig. 1(b)], the axial displacement is given by $\Delta z = -f_o^2/f_{\mathrm{F}}$, where the thin lens formula $1/f_o = 1/(-f_{\mathrm{F}} + f_o) + 1/(f_o + \Delta z)$ is used. Therefore, the 3D displacement of the focal spot

$$(\Delta x, \Delta y, \Delta z) = \left(\frac{k_X f_o}{k}, \frac{k_Y f_o}{k}, -\frac{f_o^2}{f_{\mathrm{F}}} \right) \tag{1}$$

is implemented with the phase pattern $\phi(X,Y)$ on the SLM given by

$$\phi(X,Y) = mod\left(k_X X + k_Y Y + \frac{k}{2f_{\mathrm{F}}}(X^2 + Y^2) + \pi, 2\pi \right), \tag{2}$$

where 2π is the phase modulation depth of the SLM and the constant π phase is for less phase jumping at the center.

Scaling the number of focal spots, or producing an array of optical microtraps, is achieved by generating more than one such spots simultaneously [see Fig. 1(c)]. The simplest way is to divide the SLM plane spatially and implement phase patterns onto each region; however, this scheme changes the profile of the focal spot because it loses some spatial frequencies. Alternatively, we can mix the fundamental phase patterns into a single phase pattern; each of them is randomly distributed over the entire SLM space with equal appearance. To mix N_{tr} phase patterns $\phi_m(i,j)$, where $m \in [1, N_{tr}]$ and i, j are the SLM pixel indexes, into a combined phase pattern $\phi_{\mathrm{mixed}}(i,j)$, we use an addressing matrix $S(i,j)$ of random integers between 1 and

#260694 Received 8 Mar 2016; revised 14 Apr 2016; accepted 22 Apr 2016; published 27 Apr 2016

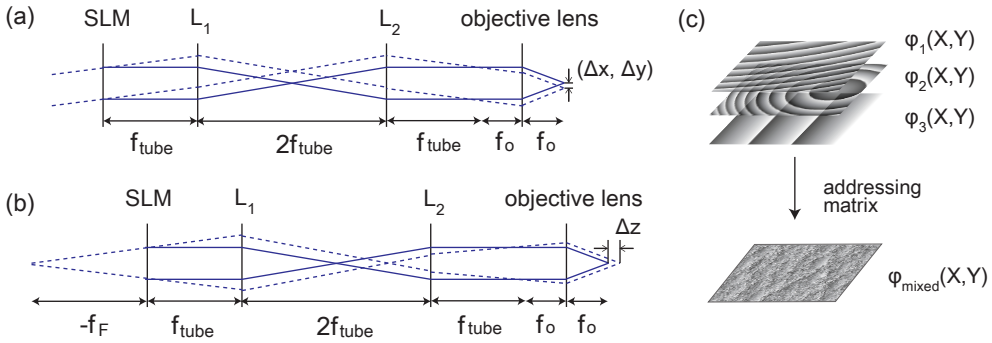

Fig. 1. (a) Transverse displacement of focal spots. (b) Axial displacement. (c) Phase pattern synthesis.

N_{tr} with an equal probability. The mixed phase pattern $\phi_{\text{mixed}}(i,j)$ is then given by

$$\phi_{\text{mixed}}(i,j) = \phi_{S(i,j)}(i,j). \tag{3}$$

In this way, each focal spot can be controlled independently while the spatial profile of the original spot is well preserved. The independent control of each focal spot guarantees the flicker-free frame-to-frame evolution of N_{tr} focal spots [22]. Note that a periodic addressing, the way in which m is chosen in a periodic manner, rather than randomly, also works, but an unwanted interference could occur.

3. Experimental procedure

In our experiment, we used cold rubidium atoms (^{87}Rb) in a magneto-optical trap (MOT) and single atoms were captured and controlled with optical microtraps (see Fig. 2). The atoms were first pre-cooled in the MOT with the D2 line (F=2 $\rightarrow$ F'=3) with a density of 10^{10} atoms/cm^3 in the vacuum chamber with a pressure of 3.0×10^{-10} Torr. The light source for the FORT was a continuous-wave Gaussian beam from a Ti:sapphire laser (SolsTiS from M-Squared Lasers) tuned at $\lambda = 820$ nm. The beam was programmed and reflected by an LCOS-SLM (Liquid Crystal on Silicon-Spatial Light Modulator, phase-only, Holoeye PLUTO, 1920×1080 pixels, 60 Hz frame rate) to generate N sub-beams. N optical microtraps were formed at the focal plane of an objective lens (Mitutoyo G Plan, $50\times$, $NA = 0.5$, working distance 13 mm, $f = 4$ mm, infinity-corrected, 3.5-mm-glass compensation), where the laser power was 0.55 W after the SLM and the beam diameter entering the obejective lens was $1/e^2 = 4$ mm, limited by the aperture size. Each sub-beam from the SLM was delivered onto the objective exit pupil by a pair of relay lenses with the same focal length of $f = 200$ mm in a 4-f geometry. The focal diameter of the sub-beam in the vacuum chamber was $2w_o = 2.28$ μm estimated by a separate beam profile measurement (not shown).

After the atoms were loaded in the MOT, the microtrap beams were turned on and the MOT cooling beam was red-shifted by 45 MHz for polarization gradient cooling (PGC) and atom imaging at the same time. After 200 ms of optical molasses, the magnetic field of the MOT was turned off to keep background atoms from further gathering. The PGC beam was temperarily turned off during axial transport of atoms in order to reduce heating. The trap depth of the microtraps was $U = (3\pi c^2\Gamma/2\omega_o^3\Delta)I > 1.4$ mK, where $\Gamma/(2\pi) = 5.75$ MHz was the natural line width of the ^{87}Rb D1 line, ω_o the transition frequency, $\Delta/(2\pi) = -1.16\times10^{13}$ Hz the detuning, and $I = 2\times10^9$ W/m^2 the intensity of the the beam. The FORT-induced heating rate

#260694 Received 8 Mar 2016; revised 14 Apr 2016; accepted 22 Apr 2016; published 27 Apr 2016

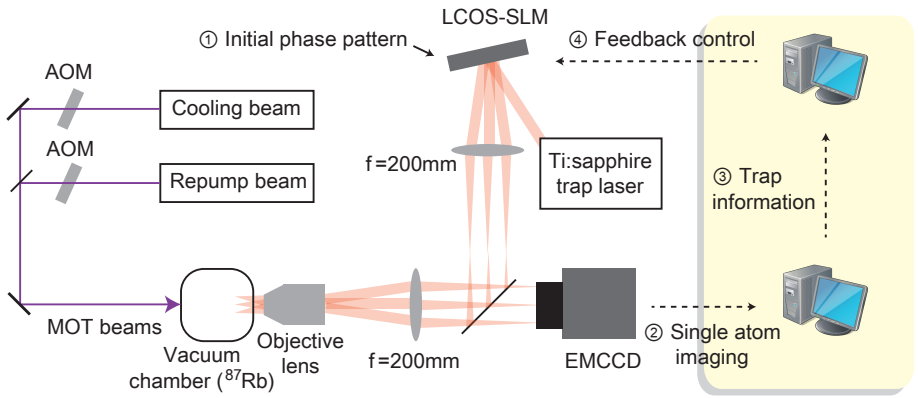

Fig. 2. Schematic illustration of the experimental setup. Optical microtraps were programmed with the LCOS-SLM to capture single atoms from the pre-cooled ^{87}Rb ensemble in the MOT. The information of the trapped single-atom configuration obtained with the EMCCD was sent back to the SLM computer for the feedback control.

was 7 μK/s assuring that the atoms remained in the cooled temperature. The trap frequency was $(2/w_0)\sqrt{U/m} \sim (2\pi)70$ kHz, where m is the mass of an atom. The fluorescence of the atoms was detected with an electron multiplied CCD (EMCCD, Andor iXon3). The EMCCD detected about 200 photons per atom during an exposure time of 50 ms. Note that the PGC scattering rate, with $I = 27$ mW/cm^2 and $\Delta \approx -17\Gamma$, was 2.9×10^5 s^{-1} and about 6.7% of emitted photons were collected with the objective lens of $NA = 0.5$. Our experiment was performed in the collisional blockade regime [13] with a single-atom trapping probability of 50.9%, measured by fluorescence histogram. The trap lifetime was $\tau > 13$ s, given from the decay of the remaining atom probability (when the trap was stationary). The decay process was dominated by background gas collisions [1].

Dynamic manipulation of the single atoms was achieved by applying a sequence of phase patterns to the SLM. We used an active area of 800×800 pixels around the SLM center to take full advantage of the hardware frame update rate of 60 fps (frames per second), because the displaying rate from the computer to the SLM was relatively slow to use the full frame. Also, we used two personal computers (PCs) to accelerate the whole operation. The phase patterns were first diagnosed with the first computer and transferred to the SLM through a display port (DVI or HDMI). In "adaptive" mode, where the set of the trap trajectories depends on the initial configuration of the atoms, the EMCCD operated by the second computer took the image of the initial atom configuration and sent the information to the first PC (see Fig. 2). The PC then loaded a 30-frame movie depending upon the initial state. For this, we prepared a look-up library having all possible trajectories between the initial and final atom configurations. The computer memory required for the look-up library in our experiment was 10 GB (gigabytes). Because each trap site was occupied probabilistically, there were total $2^{N_{tr}}$ initial configurations for N_{tr} trap sites. The memory for a single frame of 800×800 pixels with an 8-bit gray level was 640 KB (kilobytes) and there were 30 frames for each movie. So, with $N_{tr} = 9$ sites, $2^9 \times 30 \times 40$ KB was about 10 GB. During the 30-frame movie was being played on the SLM, the EMCCD captured sequential images of the atom array. The number of the movie frames was limited by the lifetime τ of the atoms.

#260694 Received 8 Mar 2016; revised 14 Apr 2016; accepted 22 Apr 2016; published 27 Apr 2016

4. Results and discussion

4.1. 2D transport demonstrations

Figure 3 shows selected demonstrations of our creation and reconfiguration of 2D single-atom arrays. In every experiment, a phase movie moved N_{tr} microtraps along each pre-defined trajectory. The phase movie frame rate was 20∼60 fps and the time interval between the captured atom images was 60 ms for the overall demonstration. The nearest neighbor spacing in arrays was $d = 4.5$ μm for every scheme of operation. In the first set of experiments, (a) rotation, (b) 2D vacancy filling, and (c) worm running in Fig. 3, the atoms were guided under a fixed scenario of placing and rearranging the N_{tr} optical microtraps. The number of trapped atoms was smaller than the number of optical microtraps, so not all optical microtraps guided atoms. So, in the second set of experiments, (d) Fall to the right: case 1, (e) Fall to the right: case 2, and (f) Fall to the right: case 3, an appropriate scenario to move the atoms was chosen from the look-up library, according to the initial configuration of the trapped atoms. Then, the microtraps occupied by atoms were guided along the chosen trajectory, while the unoccupied ones were dragged outward.

(a) Array rotation: Rotation of a 3-by-3 single atom array as a whole is presented as a simple operation on arrays. Six atoms were initially trapped out of nine optical microtrap sites and the trapping of all atoms was maintained until the end of the 150° rotation. The outermost atoms traveled a distance of 14.8 μm during the 25 operational frames which spanned 1.2 seconds. The frame-to-frame step rotation angle was 6°, so the step distance for the outermost atoms was 0.67 μm. The atoms were individually controlled in this demonstration, but rotating the phase pattern itself also worked well in our trial demonstration. Note that rotating the phase pattern rotates the focal plane profile on the axis of zeroth order diffraction beam of the SLM.

(b) Vacancy filling: A more explicit evidence of an individual atom control is demonstrated, which also could be a candidate for the vacancy filling scheme in atom arrays. Initially four atoms were captured and the atoms in diagonal sites proceeded to the next diagonal sites while the rest of the atoms stayed in their positions, ending in a complete 2-by-2 single-atom array as a whole. Despite the simplicity of the operation, it was impossible to achieve the same performance by frames generated by Gerchberg-Saxton algorithm [7], one of the widely used IFTAs, losing all the atoms only after a few frames. The traveling distance of the atoms in the diagonal sites was equal to the next nearest neighbor spacing, 6.3 μm, so the step distance in this 23-frame operation was 0.30 μm.

(c) Worm running: For another demonstration, which may be called *snake crawling*, nine atoms were initially trapped at arbitrary chosen positions and started to follow through a designated path in a line while being *pushed* by their precedent atoms (including vacancies). This scenario clearly shows a full degree of freedom in controlling the positions of individual atoms, where some atoms moved in horizontal directions and some moved in vertical directions, while the other were stationary, in a simultaneous manner. The triggering atom travels by 45 μm during 225 operational frames in 4.8 seconds. Some atoms were lost during the operation either by background gas collision or by moving loss.

(d)-(f) Fall to the right - adaptive operation: An initial 3-by-3 trap array, as in (a), trapped atoms with a probability of around 0.5 for each trap site. Since there were $N_{tr} = 9$ trap sites in the array, there were 2^9 cases of initial trap conditions. The scenario was to detect the initial positions of the atoms and move them to the right to fill the array from the right, as if they were under a gravity directing to the right. The phase pattern movie for every initial case of condition was retrieved from the look-up library. Demonstrations for three different initial condition cases are shown in (d)-(f). The feedback control, or adaptive control, worked well albeit the stationary and moving loss of the atoms. The longest travel possible was twice the nearest neighbor spacing, $2d = 9$ μm, with a step distance of 0.30 μm in the 30 operational frames.

#260694 Received 8 Mar 2016; revised 14 Apr 2016; accepted 22 Apr 2016; published 27 Apr 2016

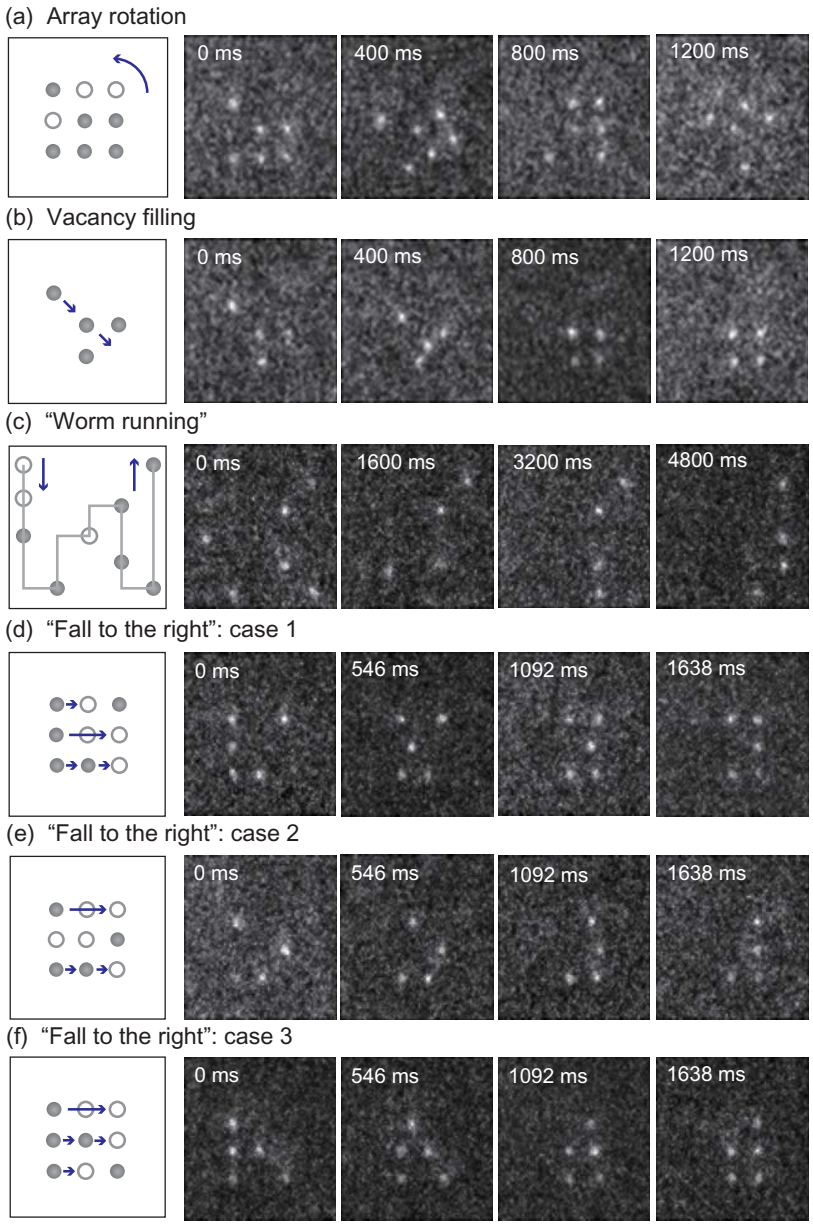

Fig. 3. Selected results of demonstration. (a) Rotation of a 3-by-3 array as a collective control. (b) 2D vacancy filling and (c) Worm running as individual atom controls. (d-f) Rightward alignment as feedback controls of atom arrays. The leftmost column presents the schematic diagram of each operation scenario. In each column, the initial and in-between photos are followed by the final photos (see Visualization 1, Visualization 2, Visualization 3, Visualization 4, Visualization 5, and Visualization 6).

#260694 Received 8 Mar 2016; revised 14 Apr 2016; accepted 22 Apr 2016; published 27 Apr 2016

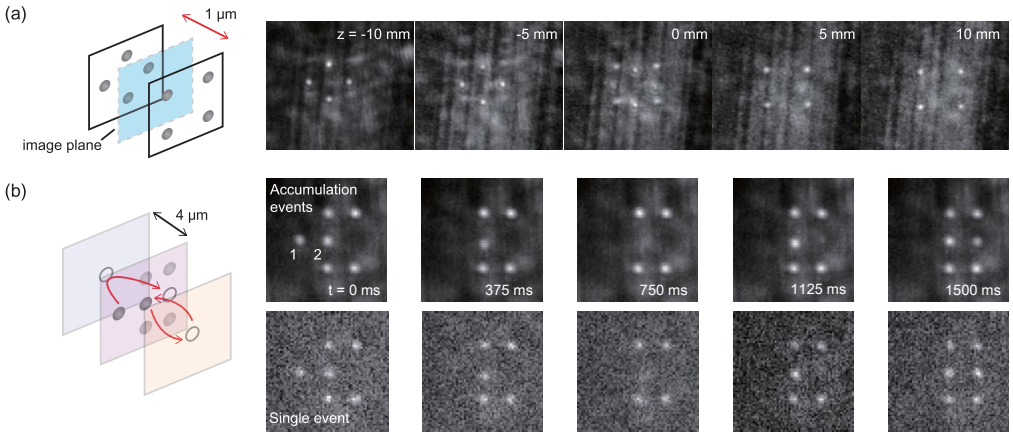

Fig. 4. (a) Trapping and imaging of a 3D single-atom array, where the image plane was shifted by translating the EMCCD. Each image corresponded to the EMCCD position at $z = -10$, -5, 0, 5, 10 mm and was accumulated from 100 single-event images that were captured right after the atoms were trapped in each acquisition. (b) Individual transport of single atoms in 3D, where each demonstration spanned 90 SLM frames and each step of atom moving was an equal division of the entire path. 370-time accumulated sequential images (the upper panel, see Visualization 7) and selected single-event sequential images (the lower panel, see Visualization 8) are displayed. The lattice constant of the 2D array was $d = 4.5$ μm and the depth of the axial travels for the both atoms were 4 μm.

4.2. *3D transport demonstration*

Finally, we present the proof-of-principle demonstration of the 3D transportation of single atoms. Fig. 4(a) shows a set of layered 2D images of a 3D atom array to check the validity of our 3D transport scheme. The 3D atom array consisted of two layers of total eight atoms. The first layer had four atoms in the square configuration and the second had also four atoms but in the diamond configuration. The layers were separated by 1 μm in the axial direction. The result in Fig. 4(a) shows the z-scan imaging of the 3D atom array conducted by translating the EMCCD in the axial direction, which confirms the creation of the 3D atom array as designed. Figure 4(b) shows a trial demonstration scheme for the 3D individual transport of single-atoms along with the captured images during the demonstration. The trial atoms moved along the designated paths out of the image plane while the other atoms stayed in position. The leftmost atom (marked as "1") was programmed to bypass the neighboring atom (marked as "2") in the axial direction to fill the vacancy in the right column. At the same time, the atom 2 traveled in the opposite axial direction. The rest atoms remained in the position during the operation. Atom 1 followed an elliptical path with the given dimensions. The SLM operated at 60 fps.

4.3. *Efficiency and loss in axial transport*

The transport efficiency of the 3D transport is shown in Fig. 5. Among $N_{tr} = 8$ trap sites initially created on the original image plane ($z = 0$), four sites were programmed to move in the positive axial direction ($\Delta z > 0$) and come back, while the other four were moved in the negative axial direction ($\Delta z < 0$) and came back. When the efficiency was defined as the ratio of the number of remaining atoms after an operation to the number of initially trapped atoms, Fig. 5(a) shows the measured efficiency for various step distances. The step distance is defined by the displacement between frames and the travel distance is the total displacement sum of the entire round-trip travel. Figure 5(b) shows the transport efficiency when the travel distance was varied and the

#260694 Received 8 Mar 2016; revised 14 Apr 2016; accepted 22 Apr 2016; published 27 Apr 2016

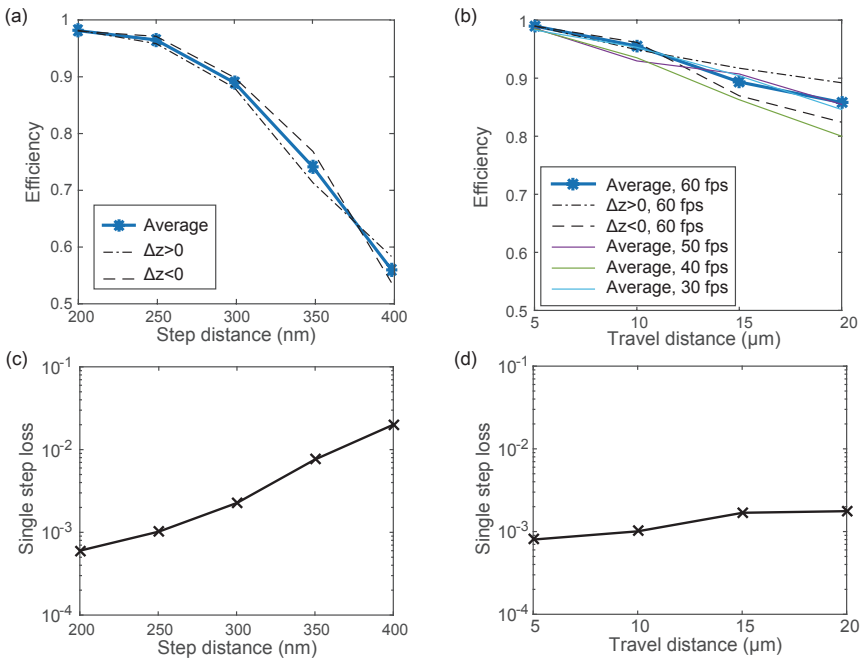

Fig. 5. (a) Single-atom transport efficiency vs. the step distance in a 40-step (41 frames) transport operation, where the values for moving in positive and negative directions are drawn with dashed and dash-dot black lines, respectively, and the total average with the blue line with 'star' marks. The given transport (only) efficiency is the actually measured probability divided by the probability without moving. (b) Single-atom transport efficiency vs. the travel distance (with a fixed step distance of 250 nm) for various frame refresh rates and directions. (c), (d) The single-step loss vs. the step distance and travel distance, calculated from the main data in (a) and (b), respectively.

step distance was fixed at 250 nm. The result shows that the transport efficiency is little dependent on the rate at which the trap is refreshed. The transport loss in a single frame-to-frame operation is calculated from Figs. 5(a) and 5(b) and the results are displayed in Figs. 5(c) and 5(d), respectively. When being calibrated with the passive loss values, the single-step transport loss increases as the step distance increases; the farther the trap moves during a frame-to-frame operation, the more the intensity flickering occurs, as expected. On the other hand, the travel distance did not increase the single step loss significantly, when the step distance was fixed, in our experiment. The results indicates that within the practical travel range of 20 μm from the initial focal plane, the traps are created in a reliable manner and, therefore, the atoms are safely transported.

We note that the main mechanism of loss from the trap is the frame-to-frame intensity flickering (degrading) which is caused by the phase jump at the boundaries of the finite SLM phase modulation range. For example, provided that the phase modulation range is $[0, 2\pi]$, a pixel evolving from 1.99π to 2.01π actually evolves from 1.99π to 0.01π, so the phase value in between has no defined value at certain time interval, failing to contribute to the trap. Note that heating and acceleration play minor roles because the scattering rate for heating is estimated to be smaller than the cooling rate, and the frame-to-frame moving speed of traps ($\sim$ 0.1 mm/s), determined by the relaxation time of the liquid crystals on the SLM, is adiabatically slow compared to the motional speed of the atoms in the traps ($\sim$ 1 m/s).

#260694 Received 8 Mar 2016; revised 14 Apr 2016; accepted 22 Apr 2016; published 27 Apr 2016

Our demonstration is currently limited by the laser power (currently up to $N = 9$ atoms), the trap lifetime ($\sim$13.4 s), the SLM update rate (60 fps), the moving loss, and the computer data communication speed, some of which can be readily improved by a new integrated system design. An operation with $N_{tr} = 25$ sites, for example, currently requires a look-up library of 660 TB (terabytes) in memory, simply exceeding the conventional PC memory capacity. Thus, a large number of atoms may be better processed with a real-time feedback generation of phase patterns, rather than using memories, which is plausible with modest graphic processing systems [24]. Also, 3D imaging of atoms in real time could be executed in a compact way with rapid 3D microscopy with tunable lenses [25].

5. Conclusions

In summary, we proposed and demonstrated a simple optical method to transport single atoms in 3D. This method utilized connected flicker-free displacements of optical microtraps to make arbitrary rearrangement paths for N atoms not only in the transverse directions but also in the axial direction. With N_{tr} optical microtraps dynamically controlled with the programmable SLM phase mask, we implemented various simultaneous and individual rearrangements of single atoms including the 2D rotation, vacancy filling, guiding, compactification, and 3D relocation of single atoms. We hope that this method of 3D atom arrangements can be useful for high-dimensional architecture operations in N-qubit quantum computations.

Acknowledgments

This research was supported by Samsung Science and Technology Foundation [SSTF-BA1301-12].

#260694 Received 8 Mar 2016; revised 14 Apr 2016; accepted 22 Apr 2016; published 27 Apr 2016